Journal of Computational Physics **162,** 395–410 (2000)
doi:10.1006/jcph.2000.6544, available online at http://www.idealibrary.com on IDEAL®

Revisiting Wall Heating

William J. Rider[1]

Hydrodynamic Methods Group, Applied Physics Division, Los Alamos National Laboratory, Mail Stop D413, Los Alamos, New Mexico 87545
E-mail: wjr@lanl.gov

Received August 19, 1999; revised May 17, 2000

The results of computing a shock reflection are found to strongly depend on the chosen coordinate system, Lagrangian or Eulerian. This is seen by comparing the amount of "wall heating" associated with the solutions to Noh's shock reflection problem computed in each reference frame. Here, an explanation is offered that places a greater burden on the role of phase error or effective wave speed in producing this effect. The reason for the greater difficulties in the Lagrangian frame are the non-uniformity of the mass coordinates in a converging geometry. This produces a non-steady-state discrete shock profile.

Key Words: shock capturing; Lagrangian; Eulerian; reflection.

1. INTRODUCTION

Shock reflection or shock interactions are often associated with a phenomenon known generically as "wall heating." This problem has been studied since the dawn of simulating shock waves [1] and has been revisited ever since [2–9]. This term was coined by Noh [5] and is most commonly associated with a shock reflecting from a wall or axis in a convergent geometry. Noh also introduced an infinite shock reflection problem that bears his name and its numerical solution is characteristic of this phenomenon. Noh's problem consists of a initial condition of a uniform density, $\rho^0 = 1$, zero pressure, $p^0 = 0$, and a uniform inflow, $u = -1$ in a unit domain $x, r \in [0, 1]$.

Typical solutions have density profiles with a large disparity from the analytical result near the axis. This is shown in Fig. 1a. Note that the Lagrangian solution experiences wall heating near $r = 0$, not present using the same method in Eulerian coordinates. The exact solution is given with the dashed line. For the Lagrangian solution, the grid is shown at the lower edge of the plot. Note that the Lagrangian grid retains the same number of cells, but

[1] This work performed under the auspices of the U.S. Department of Energy by Los Alamos National Laboratory under Contract W-7405-ENG-36.

0021-9991/00

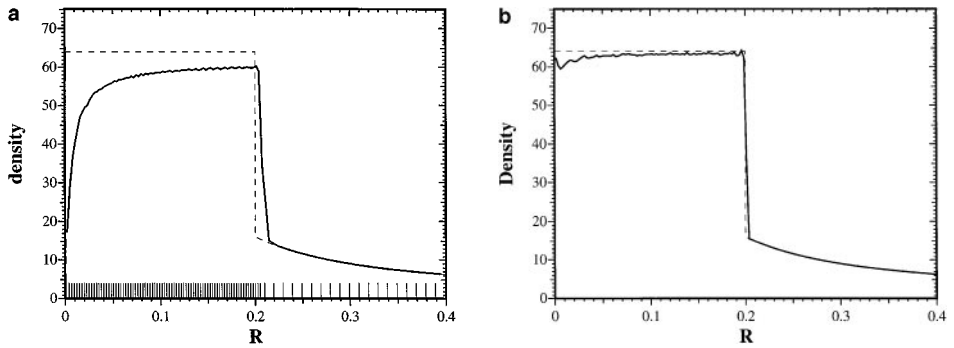

FIG. 1. Noh's problem in spherical coordinates coordinates computed using a high-resolution Godunov method. (a) Lagrangian coordinates and (b) Eulerian coordinates.

the final cell has moved from $r = 1.0$ to $r = 0.4$ due to the inflow condition. In both cases, Lagrangian or Eulerian, the solution is displayed for $x, r \in [0, 0.4]$. Comparing the shock positions in the two solutions (using linear interpolation for the spatial position where $\rho = 40$) shows the Lagrangian shock is at $r = 0.2065$ and the Eulerian shock is at $r = 0.2008$. Note that the exact shock location is $r = 1/5$. Both solutions were computed with the same Courant number, 0.8, and the same number of zones behind the shock (i.e., the post-shock state, $r \leq 0.2$) when the solution is displayed, 80. Because the pressure is computed accurately, the equation of state will provide a commensurate rise in energy (temperature) to offset the deficit in density. Hence, the term "wall heating" is used to describe these solutions.

Early studies of numerical simulations of shock waves on nonuniform meshes [3] or converging geometries [1] focused on the unsteady nature of the effective wave propagation. The problem revolves around the definition of the artificial viscosity [10, 11] defined for a steady-state shock profile and its reaction to a change in the length scale as defined by the mesh. Riemann solvers used in Godunov-type methods are based on similar principles via the Rankine–Hugoniot relations [12]. The unsteady shock propagation has not been directly related to the problem of shock reflections nor to the property of phase errors in numerical methods. Earlier studies focused on Lagrangian grids.

Here, our attention will center upon differences that manifest themselves when a calculation is done in Eulerian coordinates. Compare the results in Figs. 1a and 1b. The method used to compute these results is identical except for the frame-of-reference. It is built using the spatial and temporal differencing and Riemann solver described in [13]. Other important issues that are related to the overall interpretation of the results are the shock width, the starting errors, and the asymptotic order of the method. Each of these issues will be touched upon as the paper progresses. In the past few years, several methods have been introduced to alleviate the problems associated with this general phenomenon [9, 14]. While this effect is most acute with strong reflected shocks or symmetry boundaries, it also is important with interacting shocks [6] and contact discontinuities [15].

The motivation for this work was results that do not follow the accepted nature of the solution to Noh's problem. It is important to understand these results so that a more general and less serendipitous solution may be derived. Here we will discuss this problem and issues that expand the scope of the numerical difficulties associated with what has become known as "wall heating" beyond purely numerical dissipation to include phase errors (or nonconstant shock speed) as an important contributor to the effect in converging geometries.

First, we will present the computational evidence of the unexpected solutions to Noh's problem. We are motivated by a simple observation: for nearly identical numerical methods, wall heating is much more acute in a Lagrangian frame than it is in the Eulerian frame. In Section 3, we will offer an explanation for the observations that differ from the usual and focus on phase errors. We will present results and some predominantly heuristic reasoning that adds an important effect in the Lagrangian frame for converging geometries.

2. COMPUTATIONAL EVIDENCE

We will show results solving the Euler equations in Lagrangian coordinates,

$$\frac{\partial \tau}{\partial t} - \frac{\partial Au}{\partial m} = 0, \tag{1a}$$

$$\frac{\partial u}{\partial t} + \bar{A}\frac{\partial p}{\partial m} = 0, \tag{1b}$$

and

$$\frac{\partial E}{\partial t} + \frac{\partial Aup}{\partial m} = 0, \tag{1c}$$

in control volume form, with τ being the specific volume, $1/\rho$, u is the velocity, E is the total energy, $E = e + \frac{1}{2}u^2$, with an equation of state for the pressure, $p = (\gamma - 1)\rho e$, A the area, $\bar{A}$ is a volume averaged area, V is the physical volume, and m is the mass coordinate (ρV). We are specifically interested in the differences found in Eulerian coordinates where the Euler equations are

$$\frac{\partial \rho}{\partial t} + \frac{\partial A\rho u}{\partial V} = 0, \tag{2a}$$

$$\frac{\partial \rho u}{\partial t} + \frac{\partial A\rho u^2}{\partial V} + \bar{A}\frac{\partial p}{\partial V} = 0, \tag{2b}$$

and

$$\frac{\partial \rho E}{\partial t} + \frac{\partial A(\rho u E + up)}{\partial V} = 0. \tag{2c}$$

The main point of this paper is shown by comparing the results in Fig. 1 with Fig. 2. In Fig. 2, the solutions in the Lagrangian and Eulerian frame of reference are more alike than different and wall heat/cooling is modest at best. The exact solution is given with the dashed line. Both solutions have their largest errors at the left boundary where the shock formed and these errors are somewhat larger in the Lagrangian frame. For Noh's problem in planar coordinates, the solutions are quite similar in the two frames, while they are quite different in spherical coordinates. In both cases, the shock is sharp and is 1 zone wide. There are small oscillations in the post-shock region, and the largest errors are adjacent to the reflection boundary. The small oscillations are a result of discretely propagating a narrow, one–zone wide shock. If the Riemann solver is replaced with one that maintains a two- to three-zone-wide 2 shock, the oscillations are significantly reduced in amplitude. However, in spherical coordinates, the solutions are much different when computed using

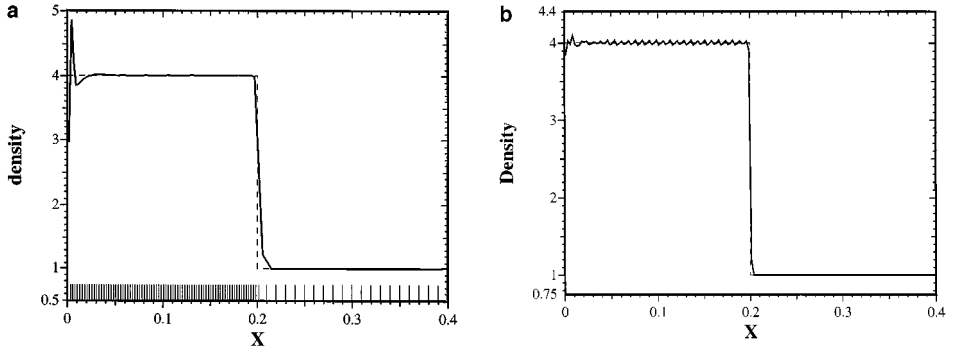

FIG. 2. Noh's problem in planar coordinates computed using a high-resolution Godunov method. (a) Lagrangian coordinates and (b) Eulerian coordinates.

the same method. The Eulerian result has very little wall heating, while the Lagrangian result is plagued by a substantial amount of wall heating. This is clear upon viewing Fig. 1.

The question to answer is why are the results in Fig. 2 so alike, while the results in Fig. 1 so different?

Conventional wisdom leads one to expect that the level of artificial viscosity is lower in the Lagrangian frame because the contact wave has been dealt with analytically rather than numerically (with dissipation) in the Eulerian frame-of-reference. One could reasonably conclude that the errors seen near $x = 0$ or $r = 0$ are starting errors. Insofar as the shock width is concerned, the high-resolution Godunov method produces a shock with a width of one zone for Noh's problem. The narrow shock is chosen to minimize the role of the shock width in determining the solution as the shock reflects from the center of the sphere. This should minimize the impact of the discrete shock width in producing pathological results [6] during the initial portion of the shock reflection.

To add to the evidence we also display the results of a modern version of an artificial viscosity method [16] in Lagrangian coordinates in Fig. 3. The solution is quite similar both qualitatively and quantitatively to the high-resolution Godunov method in Lagrangian coordinates. In this solution using the same method as used in Fig. 1, the shock is at $r = 0.2126$. One difference is that the shock computed with this method is broader, occupying three zones rather than one. The startup errors near $x = 0$ are greater in the Lagrangian solution, but are localized to several zones adjacent to the boundary. This increase in shock width also aids in reducing the post-shock oscillations.

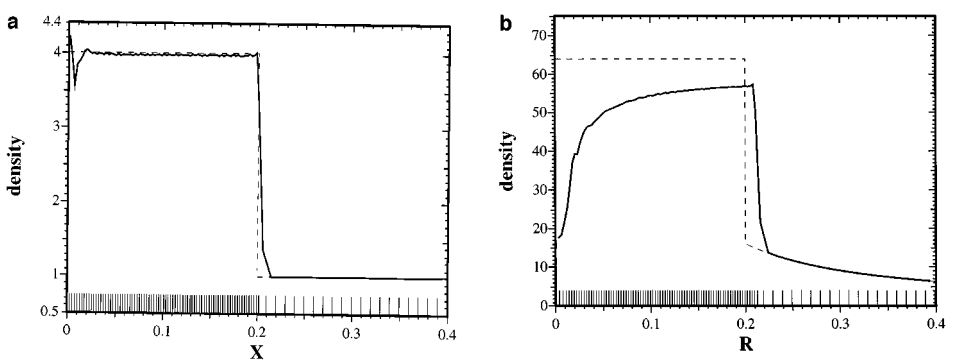

FIG. 3. Noh's problem computed with a flux-limited von Neumann-Richtmyer method for planar and spherical frames. (a) Planar and (b) spherical.

One should note two general aspects of Lagrangian solutions: the grid spacing is a dynamic variable as the solution evolves, and the mesh is described in mass coordinates in the governing equations. Thus, should one start with constant mesh spacing in planar coordinates, the constant mesh spacing will remain in mass coordinates, but the spatial mesh spacing will contract by a factor of four matching the density jump across the shock. In a one-dimensional spherical geometry the mesh spacing will also vary near the axis where the volume of mesh cells changes dramatically (with constant radial spacing). In spherical geometry, the ratio in volume between the first and second control volumes is 1 : 7. Between the second and third control volumes the ratio is nearly 1 : 3. Thus, the mass of zones changes dramatically near the center of the sphere, resulting in a highly variable mesh spacing. One is confronted with variable coordinate spacing in general and, in convergent geometries, variable mesh spacing in both spatial and mass coordinates. This is further exaggerated by the compression of mesh cells across the shock.

A cautionary note should be taken when comparing Lagrangian and Eulerian solutions. Some Eulerian codes are solved using an internal energy equation rather than the total energy equation [7, 17–19]. The internal energy equation is an evolution equation, while the total energy equation is a conservation equation. At this point it is important to note that convergence to a weak solution of the Euler equations is assured by the use of discretely conservative difference schemes [20, 21]. Therefore, the solutions found using the internal energy equation are not certain to converge to a weak solution of the Euler equations. We also note that the von Neumann–Richtmyer code uses the internal energy equation although modern methods based on compatible differencing [22] produce conservation of energy at a discrete level, and thus should converge to a weak solution. The unique weak solution is found through an adequate amount of entropy production.

Solutions in Eulerian coordinates using the internal energy equation are susceptible to "wall heating" errors that seem reasonable given the nature of solutions in the Lagrangian coordinates. In our code, the energy equation is modified from (2c) to

$$\frac{\partial \rho e}{\partial t} + \frac{\partial A \rho u e}{\partial V} + p\frac{\partial A u}{\partial V} = 0,$$

purely for the purpose of updating the energy from old to new time levels. Results using this equation are shown in Fig. 4 where wall heating is evident in the spherical Noh problem.

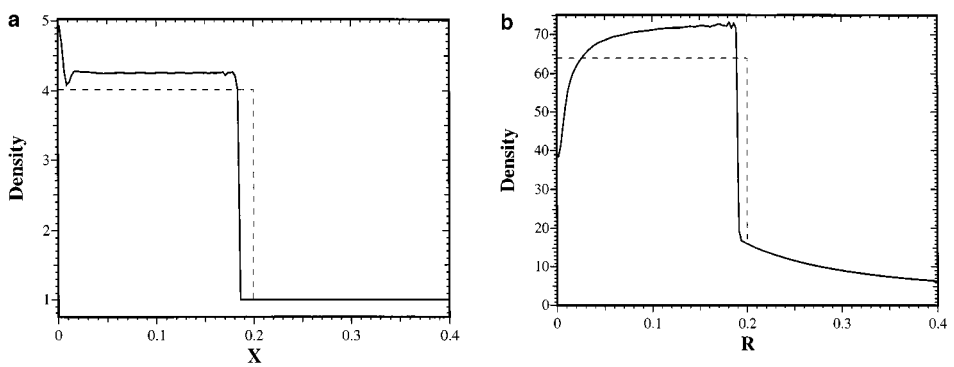

FIG. 4. Noh's problem solved in Eulerian coordinates with a high-resolution Godunov method, which updates the internal rather than the total energy equation. (a) Planar and (b) spherical.

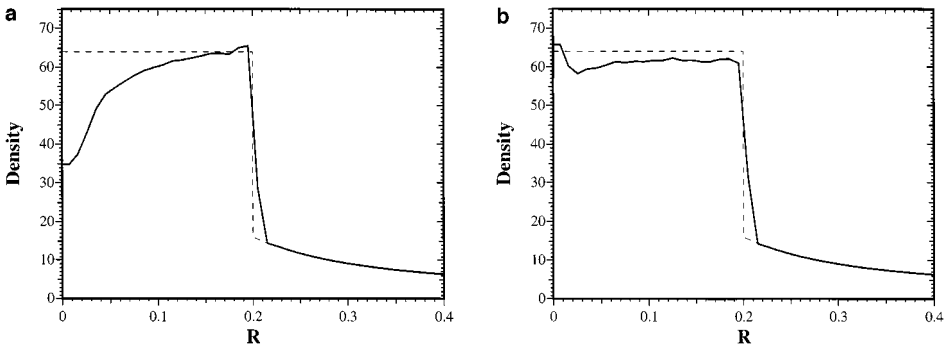

FIG. 5. The solution to Noh's problem using the internal energy equation, but with 100 zones (only 20 in the post-shock state). (a) Internal energy with 100 zones and (b) total energy with 100 zones.

The solution converges to an incorrect answer in both cases. These calculations are done using the same numerical conditions (zone number and CFL number) as Figs. 1b and 2b. One should recognize that the code used to solve Noh's problem is identical to the code used in the other Eulerian results except for the form of the energy equation used to update the cell-centered variables (i.e., the same time and space differencing and Riemann solver).

Furthermore, the results both indicate that the solution is converging to an incorrect answer with a density that is too high and a shock speed that is too low. Additionally these aspects are masked by the wall heating, which produces solutions that do not show the overshoot in the density if the calculation is conducted on coarser grids (as is the common practice for Noh's problem). This result is given in Fig. 5 where the solution is similar to those seen in Lagrangian coordinates. Note that this solution seems reasonable or even high-quality given the Lagrangian results in Fig. 1a or Fig. 3b. Without using mesh refinement to study the convergence of the solution, the problems seen at higher mesh resolution escapes notice. For comparison the total energy solution with 100 zones is also shown. Similar results have been shown in [19]. On the other hand, the use of adaptive grids and implicit time integration with an internal energy equation can lead to impressively accurate solutions to Noh's problem [7]. Another caveat is that Lagrangian frame solutions found with artificial viscosity formulations typically employ an internal energy equation, but converge experimentally to the correct solution of the Noh problem.

Returning to our original computations, the results are viewed in a somewhat different manner in Fig. 7. First, the planar calculations will be compared through the evolution of entropy errors and the density in the cell adjacent to the boundary. This is displayed in Fig. 6. The entropy errors are largest during the startup of the shock, but settle down and become fairly small as time progresses. The Lagrangian schemes have larger relative errors than the Eulerian. In planar coordinates, the Eulerian and Lagrangian schemes are more similar than different. Here, the entropy comparison is given by the ratio of the computed entropy and the analytical solution,

$$\text{Ratio of Entropy Error} = \frac{\sum_i V_i\, p_i\, \rho_i^{(1-\gamma)} - 2^{2/3} t/9}{2^{2/3} t/9},$$

where V_i is the volume of a mesh cell ($\sum_{\text{exact}} V = x_{\text{exact}}$, $x_{\text{exact}} = st$, $s = 1/3$, $p_{\text{exact}} = 4/3$, $\rho_{\text{exact}} = 4$). The errors are quite comparable between the methods although the Eulerian

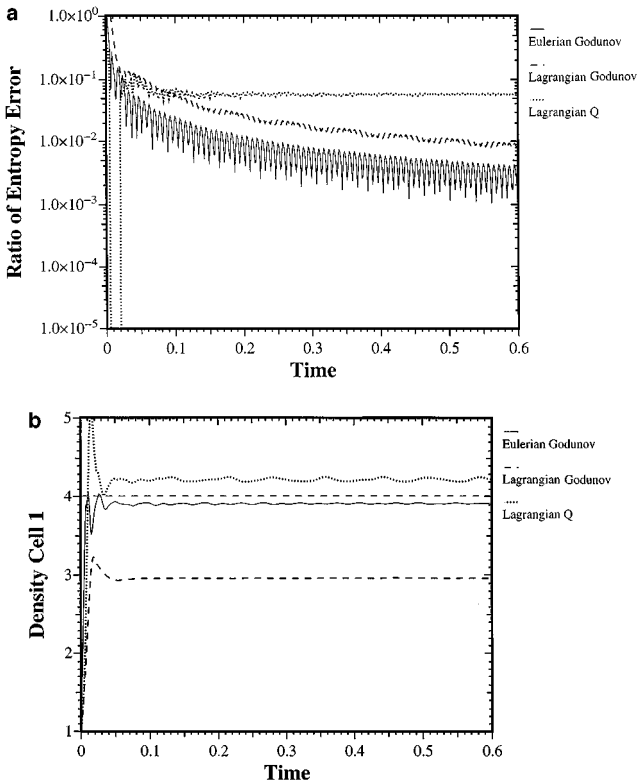

FIG. 6. A comparison of relative entropy errors for three solutions to Noh's problem in planar coordinates. The density in the first computational cell (adjacent to the reflecting boundary) is also displayed. (a) Entropy error and (b) density in cell 1.

solution has somewhat smaller errors. In the case of the density in the first zone, the Lagrangian solution is comparable to the the Eulerian solution. Interestingly, the artificial viscosity code produces an overshoot in velocity in the first zone.

Next, we will compare the spherical case's numerical solution in the same fashion. As with the planar case, the entropy comparison uses the difference between the analytical and numerical solution,

$$\text{Ratio of Entropy Error} = \frac{\sum_i V_i\, p_i \rho_i^{(1-\gamma)} - 16\pi t^3/243}{16\pi t^3/243},$$

where V_i is the volume of a mesh cell ($\sum_{\text{exact}} V = 4/3\pi r_{\text{exact}}^3$, $r_{\text{exact}} = st$, $s = 1/3$, $p_{\text{exact}} = 64/3$, $\rho_{\text{exact}} = 64$). By comparing the relative entropy errors in Fig. 7a one can see that the Eulerian frame solution has the smallest production of entropy once the initial shock is formed. Both of the Lagrangian frame solutions have higher entropy production although the artificial viscosity method is the least dissipative at the outset of the solution. This seems counter to the conventional wisdom mentioned above. It is interesting to recognize that the magnitude of the entropy error is roughly proportional to the error in the shock position.

The density in the first cell behaves in a fundamentally different fashion depending on whether one computes the solution in the Eulerian or Lagrangian frame for the convergent geometry. As shown in Fig. 7b, the density in the Eulerian frame overshoots the analytical

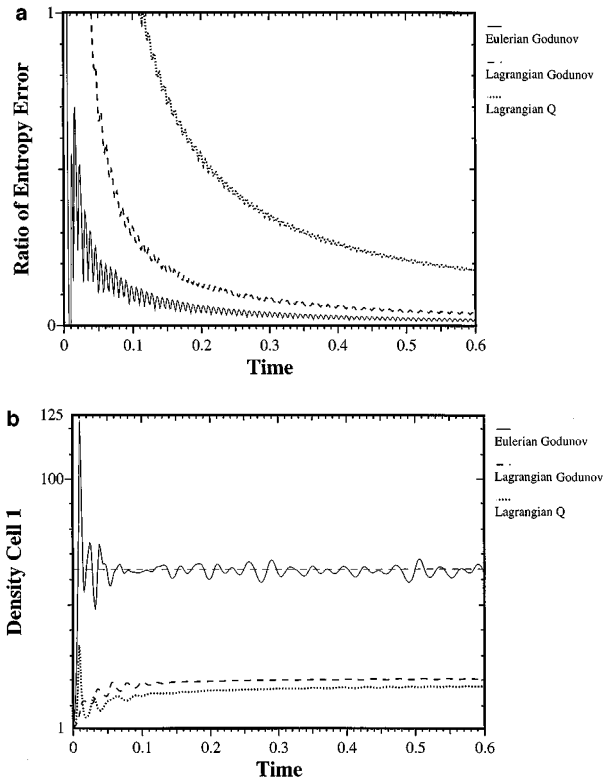

FIG. 7. A comparison of relative entropy errors for three solutions to Noh's problem in spherical coordinates and the density in the first computational cell (adjacent to the axis). (a) Entropy error and (b) density in cell 1.

answer initially, then oscillates around the correct value. The entropy errors are enormous during the startup of the shock, but settle down as time progresses. The Lagrangian schemes have larger relative errors than the Eulerian. The Eulerian and Lagrangian schemes are fundamentally different in the density evolution. This becomes clearer upon viewing the close-up on the initial shock reflection in Fig. 8. Generally, the entropy startup errors are larger with the two Godunov methods, but fall below the more classical artificial viscosity method quickly. The difference in the Eulerian frame is the large overshoot in density as the shock forms on the grid. This may be associated with a brief period where insufficient entropy is produced by the method. The exact solution is plotted on the density plot for reference. The overshoot in the density in the Eulerian frame is associated with too little entropy production. The "bump" in the plot indicates where the entropy errors are negative.

This will be further elaborated upon below, indicating that the shock wave speed will be under predicted in this case, also indicative of lower than analytic entropy production. One should recognize that too little dissipation is produced. By using a slightly more dissipative method, the size of the error can be reduced (i.e., a minmod limiter or a Lax–Friedrichs-type [14] or HLLE Riemann solver [23]). In the Lagrangian frame the density does not reach the analytical result at any time and levels out to a smaller value. In the Eulerian frame the density rises rapidly and overshoots the analytical solution, then oscillates near the analytical solution at late times. The overshoot in Eulerian coordinates closely corresponds to the time when the entropy produced does not exceed the analytical result.

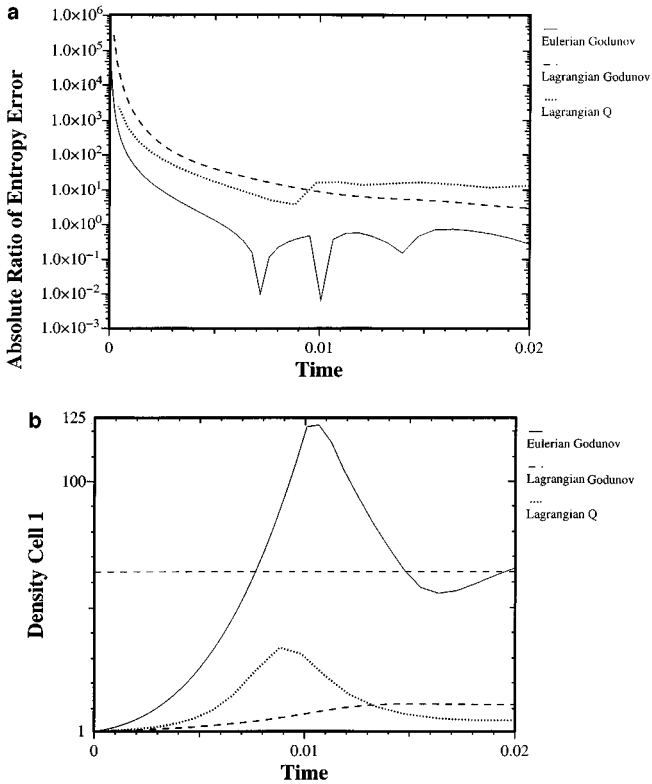

FIG. 8. A comparison of relative entropy errors for three solutions to Noh's problem in spherical coordinates in the initial formation of the reflected shock. The density in the first computational cell (adjacent to the axis) is also displayed. (a) Entropy error and (b) density in cell 1.

Ralph Menikoff has observed a structured explanation for the values that the Lagrangian calculations produce in the first zone for a spherically convergent geometry [24]. Spherical convergence creates a rise in density of 16 solely through isentropic compression. Through the equation of state this would drive a pressure rise of 16 as well. Note that in Noh's problem the initial pressure is identically zero. In an isentropic process, $(\rho_1/\rho_2) = (p_1/p_2)^{1/\gamma}$; thus combined with the initial jump density of 4 due to shock compression this leads to a density slightly larger than 21 ($4 \cdot 16^{3/5}$). All of the Lagrangian solutions are consistent with this prediction (Figs. 1a and 3b). On the other hand, the Eulerian calculations are not. This would lead one to believe that the Lagrangian methods treat the initial shock reflection in a more isentropic manner than the Eulerian ones. This receives some support by noting the size of the initial entropy errors committed by each scheme.

This may have significant bearing on steps that can be taken to ameliorate the effects of the phenomena. Noh suggests adding artificial heat conduction to reduce the impact of wall heating [5]. This is discussed in a more modern context in [8] near the end of their paper. Other manners of addressing this issue are to use grids where the zoning matches cell masses or impedance ($\rho c V$; c is the sound speed). Within the context of Godunov methods, approximate Riemann solvers that smear the contact wave (such as Lax–Friedrichs taken generally) will have this property. Note that the velocity behind the shock is analytically zero although typically numerical solutions will oscillate around zero (in connection with

weak shocks bouncing off of the wall or axis). We will return to this question later and view this in a new light given the following discussion.

3. AN EXPLANATION

It is useful to comment on the nature of dissipation in linear and nonlinear partial differential equations at this point. In any case, some terms must be added to the inviscid equations to produce dissipation as required for physically relevant solutions by the second law of thermodynamics, $TdS \geq 0$. The terms introduced into the Euler equations to satisfy the second law of thermodynamics can also be viewed as a necessary regularization of the equations for weak solutions. Following from classical analysis (Fourier or modified equation), in linear equations these terms are exclusively even order differential terms, while the odd order terms produce phase errors. For nonlinear equations the precise nature of dissipation is significantly cloudier with differential terms of either order producing the dissipation or dispersion. An example where odd-order terms are considered as having both characters is found in [25, 26]. In general, the modified equations have proven useful for explaining the properties of first-order monotone methods [27], and second-order methods [28]. The continuum behavior of the modified equation provides significant explanatory insight into the discrete behavior of approximations.

Lack of clarity not withstanding, errors in the speed of wave propagation can produce errors in dissipation. Too large a shock speed will result in excess dissipation. This impact has been seen in Fig. 7a where the Lagrangian frame dissipation exceeds that of the Eulerian frame. There the mass coordinates' growth as r increases produces an expanding grid and a commensurate phase error. As shock strength increases, dissipation is increasingly dominated by terms that can be viewed as third-order through the expansion for wave speed,

$$W = \rho(c - s\Delta u),$$

where c is the sound speed, $s = (\gamma + 1)/4$ in the weak shock limit, where $|\Delta u| \ll c$, and $s = (\gamma + 1)/2$ in the strong shock limit, where $-\Delta u \gg c$. It is the strong shock limit and the above asymptotics that motivated the nonlinear form chosen by von Neumann and Richtmyer [10], which has the effective differential form,

$$Q \sim \frac{\partial}{\partial x}\left(\left|\frac{\partial u}{\partial x}\right|\frac{\partial u}{\partial x}\right),$$

a third-order positive definite dissipative term [25, 26, 29].

An example of this effect in a Godunov-type integrator can be fashioned for computing the momentum flux in Lagrangian coordinates,

$$p_{LR} = \frac{1}{2}(p_l + p_r) - \frac{1}{2}|\lambda|(u_R - u_L)$$

where L and R correspond to the left and right states, LR to the interface state, and λ is an estimate of the wave speed. Inserting the above values for the wave speed, $\lambda = \rho(c - s\Delta u)$, one can see that the first term leads to a linear diffusion-like term, but the second term (proportional to s) will lead to something similar to the form chosen by von Neumann and Richtmyer when the flow is compressing [30].

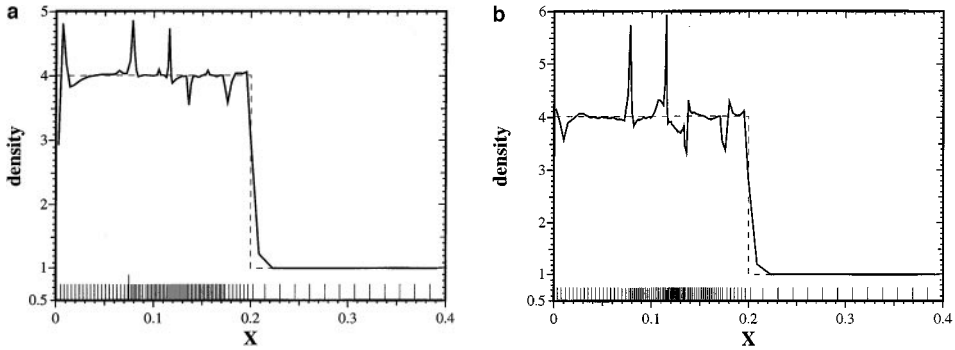

FIG. 9. The effect of a shock running through a mesh transition where the mesh goes from a coarser to a finer spacing and then a finer to a coarser spacing. (a) High-resolution Godunov method and (b) von Neumann-Richtmyer.

As alluded to above, differences in the solution between the Lagrangian and Eulerian frames can be attributed to the fixed mass nature of cells for the Lagrangian frame of reference. When a Lagrangian cell is shocked and compressed its spatial extent must shrink. This causes a shock to move from a fine mesh into a coarser one. This is ameliorated to some extent by the tendency for first-order differencing to be chosen by monotonicity constraints near the shock. For the Lagrangian code in planar coordinates, this causes problems for the spatial differencing, as the mesh spacing is intrinsically unequal. In spherical coordinates, the mass of zones with equal radial spacing is acutely different near the center of a sphere. As noted earlier, the ratio in mass between the first and second zones is $7:1$. This further exacerbates the problem of mesh variation due to compression across the shock especially near the axis.

To further focus the attention on mesh variation consider a planar shock crossing the boundary between a coarser to a finer mesh and back from a finer to coarser mesh. A computed solution is shown for two $2:1$ mesh variations in Fig. 9. The problem is set up as follows in order starting at $x = 0$, 20 zones with $\Delta x = 1/65$, 20 zones with $\Delta x = 1/130$, 20 zones with $\Delta x = 1/260$, 20 zones with $\Delta x = 1/130$, and 20 zones with $\Delta x = 1/65$. Woodward used a similar problem in [31] showing the same qualitative effects.

The calculations shown in Fig. 9 are compelling evidence that variations in mesh spacing can have a profound impact on the solution mimicking the errors found in spherically converging geometries. This shows that "wall heating" occurs precisely where the mesh is increasing its spacing and grows worse as the size of the mesh variation grows. Indeed, we can refer to this as "mesh heating." Conversely, the solution experiences "mesh cooling" where the mesh is refined. Note how the solution gives the effect of wall heating at the point of mesh expansion and the impact of the mesh variation under refinement is to "cool" the solution, resulting in a rise in density. One should also compare Fig. 9a with Fig. 2a and Fig. 9b with Fig. 3a to judge the severity of the errors induced by the variable grid.

One can also make a general heuristic explanation of the basic mechanisms at work with a variable mesh. As the mesh spacing changes from small to large a leading phase error causes the shock to propagate too fast leaving a deficit of material in its wake. This deficit contributes greatly to "wall heating" as a property of the solution. Extending on this heuristic line-of-thought, in a control volume scheme a wave passing to a coarser mesh will experience an acceleration through the averaging. This gives a wall heating effect where the mesh moves from a finer to a coarser grid spacing.

One is then led to ask what happens if the opposite case is found where the mesh is shrunk where a shock passes? Our analysis leads us to believe that the wave will slow down due to shrinking propagation velocity. This slowing will cause a "wall cooling" effect that is observed in the calculations shown in Fig. 9.

A notable aspect of this phenomena is discussed as it pertains to adaptive mesh refinement [32]. If a shock is allowed to cross the boundary between meshes of different resolution, numerical pathologies arise. This connection reminds one that the problem has an analytical explanation in the nature of phase error. Phase error is dispersive and typically the leading order error for a second-order method. This error is often larger for small Courant numbers. If there is a constant (not proportional to the Courant number) in the expression for the phase error, it will become quite significant should the errors be integrated to a fixed time where the error will become proportional to number of time steps rather than the size of the time steps.

Information will be propagated along characteristic directions. In the one-dimensional Euler equations there are three characteristics, two acoustic (genuinely nonlinear) and the material velocity (linear degenerate contact discontinuity). The time step is chosen by the largest characteristic speed, which is associated with one of the acoustic modes. Therefore, information propagating along other characteristics will be integrated at lower effective Courant numbers. As noted earlier, the material velocity behind the shock is nearly zero and therefore the material velocity Courant number will be nearly zero. Errors made in propagating information at small Courant numbers will influence the solution in the post-shock region. Noting the form of the characteristic variables further bolsters our claim. The acoustic characteristic variables are $\Delta p/c \pm \rho \Delta u/c^2$, which is observed to be small behind the shock, while the contact characteristic variable, $\Delta \rho - \Delta p/c^2$, is large. This further points to the behavior of the material wave being the key to the post-shock errors in Noh's problem. Next, it will be shown that two "building block" schemes have fundamentally different properties that may significantly influence the results observed. These differences are most acute in the expressions as the Courant number goes to zero.

Now let us consider the effect of Lax–Friedrichs-type differencing on Noh's problem. Fig. 10 shows the impact of using a Lax–Friedrichs-type method as an approximate Riemann solver [33]. It is notable that the wall heating is nearly absent from the solution. The analysis that follows uses Fourier analysis and the modified equation of each method on the linear wave equation, $v_t + a v_x = 0$ with an expansion for amplitude and phase errors. Assuming

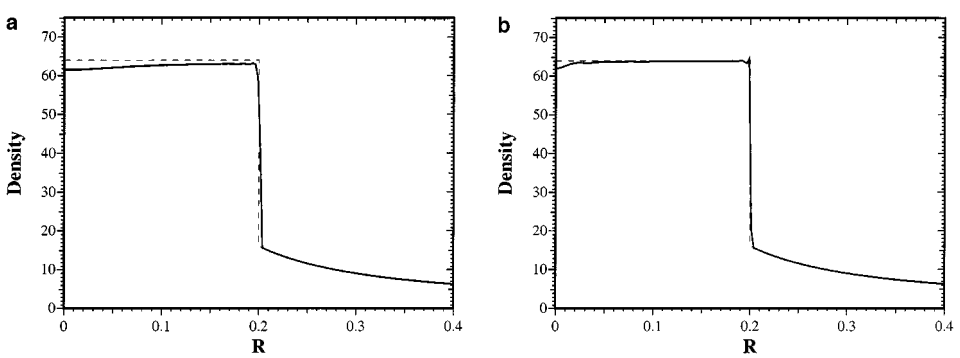

FIG. 10. Noh's problem in spherical coordinates coordinates with first-order and second-order Godunov Method and a HLL Riemann solver (like Lax-Friedrichs). (a) First-order and (b) second-order.

that $a > 0$ for simplicity, the upwind method is simply

$$v_j^{n+1} = v_j^n - \nu\left(v_j^n - v_{j-1}^n\right),$$

where $\nu = a\Delta t/\Delta x$ and the Lax–Friedrichs method is

$$v_j^{n+1} = v_j^n - \nu\left(v_{j+\frac{1}{2}} - v_{j-\frac{1}{2}}\right),$$

where

$$v_{j+\frac{1}{2}} = \frac{1}{2}\left(v_j^n + v_{j+1}^n\right) - \frac{1}{2\nu}\left(v_{j+1}^n - v_j^n\right).$$

If one looks at the basic nature of the discrete errors, it is important to note that amplitude errors never vanish for Lax–Friedrichs, $E_{\text{amp}} = 1 - \frac{1}{2}(1-\nu)\theta^2$, while they do for upwind differencing, $E_{\text{amp}} = 1 - \frac{1}{2}\nu(1-\nu)\theta^2$ where $\theta \to 0$ is the wavenumber (making the expansions formally valid for long wavelength perturbations). In terms of the modified equation, Lax–Friedrichs produces a second-order term

$$\frac{\Delta x^2}{2\Delta t}(1-\nu^2)\frac{\partial^2 u}{\partial x^2},$$

while upwind differencing gives

$$\frac{\Delta x^2}{2\Delta t}(\nu-\nu^2)\frac{\partial^2 u}{\partial x^2}.$$

Both Fourier analysis and the modified equations give the same forms and provide the same conclusion regarding the $\nu \to 0$ behavior. Lax–Friedrichs differencing remains dissipative as the Courant number goes to zero, while upwind differencing's dissipation vanishes as the Courant number goes to zero.

One might conclude from this that as the Courant number goes to zero the phase error of upwind scheme begins to dominate the solution. The Fourier analysis based phase errors for the two schemes have similar form, $E_{\text{phase}} = 1 + (-\frac{1}{6} + \frac{1}{2}\nu - \frac{1}{3}\nu^2)\theta^2$ for the upwind, and $E_{\text{phase}} = 1 + (\frac{1}{3} - \frac{1}{3}\nu^2)\theta^2$ for Lax–Friedrichs. In terms of the modified equations, the third-order dispersive terms are the same for each method,

$$\frac{\Delta x^3}{6\Delta t}(-\nu+\nu^3)\frac{\partial^3 u}{\partial x^3}.$$

One could be led to conclude that in the limit of small Courant numbers, as is the case in the material velocity in the post shock region of Noh's problem, the upwind method is dominated by the leading phase errors, while the Lax–Friedrichs method continues to be dominated by dissipative errors.

Given the results in Fig. 10 where a more viscous method shows reduced wall heating over the assumed less viscous upwind method, while both methods produce nearly equal dissipation for acoustic waves, the Lax–Friedrichs class of methods (such as HLL) produce much more dissipation on the material wave. This excess dissipation is proportional to the ratio of acoustic wave speeds to the material velocity, demonstrating that where viscous effects remain on the contact wave the wall heating is largely absent from the solution. It

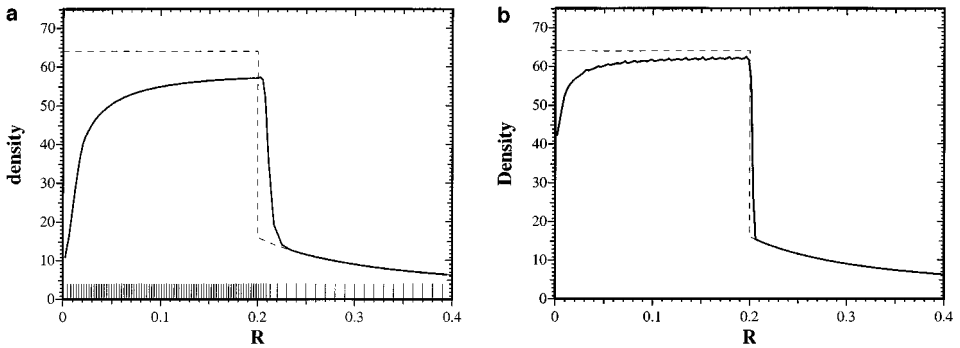

FIG. 11. Noh's problem is spherical coordinates coordinates computed using a first-order Godunov Method using the two-shock Riemann solver. (a) Lagrangian coordinates and (b) Eulerian coordinates.

is this point that has a connection with the artificial heat conduction cure for wall heating proposed by Noh [5]. Compare the first-order results in Fig. 11b with Fig. 10a. In general, the results with the first-order HLL solver is much superior in virtually every respect to the assumed lower viscosity method.

By computing the entropy in each case, the actual dissipation can be discussed. When comparing the entropy error in the spherically convergent case, the HLL method has an error nearly three times lower than the assumed less dissipative upwind method. This result shows that the production of entropy is more complex in the nonlinear case than linear analysis suggests. The greater phase error and lower assumed errors result in a larger actual error. It should be noted that much of this result is dependent upon solving a problem in the strong shock limit. This points to viscosity generally reducing the wall heating, while phase errors would be indicated as the cause of the error. More generally this would indicate that controlling phase error may have more impact on the reduction of wall heating than dissipation. This explanation is contrary to accepted notions.

This work does not claim that the wall heating error is all phase error, but rather that its origins are more complex than commonly thought. Dissipative errors associated with first-order discretizations (or even-order) errors are still present and contribute strongly to the overall effect. One should compare the results in Fig. 11 with those in Fig. 1 to see how comparable first- and second-order methods compute this problem, demonstrating the greater similarity in solutions where viscosity dominates the solution. Generally, going from a second-order to a first-order method causes some increase in the severity of the problem in the Lagrangian frame. In the Eulerian frame, the opposite effect is seen. In the Eulerian frame, first-order differencing produces results that would be expected to be similar to those used to Lagrangian frame results. Quantitatively, the errors reduce from 0.294 to 0.163 in the Lagrangian frame and 0.0701 to 0.0231 in the Eulerian frame (a volume weighted sum of density errors behind the shock). The shock position improves from $r = 0.2102$ to $r = 0.2065$ in the Lagrangian frame and $r = 0.2027$ to $r = 0.2008$ in the Eulerian frame (shock position defined by a density of $\rho = 40$, its exact solution is $r = 0.2000$). In the Lagrangian frame second-order differencing improves the results by less than a factor of 2, while in the Eulerian frame the improvement is by more than a factor of 3. To bolster our analysis, we find counter-intuitive results with respect to the choice of approximate Riemann solvers. For first-order differencing, the HLL-class of solvers produces much less dissipation than an upwind method in the spherically convergent Noh problem.

4. SUMMARY

The problem of wall heating has been an issue for as long as shock physics calculations have been performed. When a calculation is done in a converging geometry, the Eulerian calculations using a conservative differencing method shows distinctly less wall heating than comparable solutions in the Lagrangian frame. An explanation has been proposed that places a greater emphasis on the effective shock speed than the purely dissipative properties of the regularization chosen for the Euler equations.

Our evidence begins with consistent differences between the Lagrangian and Eulerian frame solutions. Another piece of conclusive evidence are the differences found with first-order Godunov methods. Using Riemann solvers with intrinsically different properties for dissipation and phase error in the limit of small Courant number, we produce results that can be explained via analysis of the methods as applied to the linear wave equation. For first-order differencing, the more diffusive method (HLL) produces results with less wall heating (lower entropy errors), while the less diffusive upwind method produces large wall heating effects (larger entropy errors). The upwind method produces its wall heating errors when its error is dominated by phase error. Finally, the effects of embedded mesh refinements can reproduce both wall heating and its opposite. These mesh refinements errors are most often associated with phase error. These effects are consistent with our explanation of the reason for enhanced wall heating in the Lagrangian frame because of the nature of mass coordinates.

ACKNOWLEDGMENTS

Ralph Menikoff's discussion of this paper in general and his physical explanation for wall heating was both stimulating and appreciated. Ed Caramana provided a number of references of historical significance on early observations of wall heating and a discussion of artificial viscosity. We would like to thank a number of people for their insightful comments on various drafts of this paper: Vince Mousseau, Rob Lowrie, Len Margolin, and Jim Kamm. Last, we appreciate the efforts of the anonymous referees whose efforts have improved this paper greatly.

REFERENCES

1. R. E. Peierls, *Theory on von Neumann's Method of Treating Shocks.* Technical Report LA-332 (Los Alamos Scientific Laboratory, 1945).
2. R. Landshoff, *A Numerical Method for Treating Fluid Flow in the Presence of Shocks.* Technical Report LA-1930 (Los Alamos Scientific Laboratory, 1955).
3. I. G. Camerson, An analysis of the errors caused by using artificial viscosity terms to represent steady-state shock waves, *J. Comput. Phys.* **1**, 1 (1966).
4. L. G. Margolin, H. M. Ruppel, and R. B. Demuth, Gradient scaling for nonuniform meshes, in *Numerical Methods in Laminar and Turbulent Flow* (Pineridge Press, Swansea, UK, 1985).
5. W. F. Noh, Errors for calculations of strong shocks using an artificial viscosity and an artificial heat flux, *J. Comput. Phys.* **72**, 78 (1987).
6. R. Menikoff, Errors when shock-waves interact due to numerical shock width, *SIAM J. Sci. Comput.* **15**, 1227 (1994).
7. M. Gehmeyr, B. Cheng, and D. Mihalas, Noh's constant-velocity shock problem revisited, *Shock Waves* **7**, 255 (1997).
8. E. J. Caramana, M. J. Shashkov, and P. P. Whalen, Formulations of artificial viscosity for multi-dimensional shock wave computations, *J. Comput. Phys.* **144**, 70 (1998).
9. R. P. Fedkiw, A. Marquina, and B. Merriman, An isobaric fix for the overheating problem in multimaterial compressible flows, *J. Comput. Phys.* **142**, 545 (1999).

10. J. VonNeumann and R. D. Richtmyer, A method for the numerical calculation of hydrodynamic shocks, *J. Appl. Phys.* **21**, 232 (1950).
11. R. D. Richtmyer and K. W. Morton, *Difference Methods for Initial Value Problems* (Wiley–Interscience, New York, 1967).
12. E. F. Toro, *Riemann Solvers and Numerical Methods for Fluid Dynamics* (Springer-Verlag, Berlin, New York, 1997).
13. W. J. Rider, An adaptive Riemann solver using a two-shock approximation, *Comput. Fluids.* **28**, 741 (1999).
14. R. Donat and A. Marquina, Capturing shock reflections: An improved flux formula, *J. Comput. Phys.* **125**, 42 (1996).
15. R. P. Fedkiw, T. Aslam, B. Merriman, and S. Osher, A non-oscillatory Eulerian approach to interfaces in multimaterial flows (the ghost fluid method), *J. Comput. Phys.* **152**, 457 (1999).
16. D. J. Benson, Computational methods in Lagrangian and Eulerian hydrocodes, *Comput. Methods Appl. Mech. Eng.* **99**, 235 (1992).
17. R. L. Bowers and J. R. Wilson, *Numerical Modeling in Applied Physics and Astrophysics* (Jones, Bartlett, Boston, 1991).
18. J. M. Stone and M. L. Norman, ZEUS-2D: A radiation magnetohydrodynamics code for astrophysical flows in two space dimensions. I. The hydrodynamic algorithms and tests, *Astrophys. J. Suppl. Ser.* **80**, 753 (1992).
19. J. R. Buchler, Z. Kollath, and A. Marom, An adaptive code for radial stellar model pulsations, *Astrophys. Space Sci.* **253**, 139 (1997).
20. P. D. Lax and B. Wendroff, Systems of conservation laws, *Comm. Pure Appl. Math.* **13**, 217 (1960).
21. R. J. Leveque, *Numerical Methods for Conservation Laws* (Birkhäuser, Basel, 1990).
22. E. J. Caramana, D. E. Burton, M. J. Shashkov, and P. P. Whalen, The construction of compatible hydrodynamics algorithms utilizing conservation of total energy, *J. Comput. Phys.* **146**, 227 (1998).
23. B. Einfeldt, On Godunov-type methods for gas dynamics, *SIAM J. Numer. Anal.* **25**, 294 (1988).
24. R. Menikoff, personal communication, 1999.
25. B. T. Hayes and P. G. LeFloch, Nonclassical shocks and kinetic relations: Scalar conservation laws, *Arch. Rat. Mech. Anal.* **139**, 1 (1997).
26. P. G. LeFloch and R. Natalini, Conservation laws with vanishing nonlinear diffusion and dispersion, *Nonlinear Anal. Theory Methods Appl.* **36**, 213 (1999).
27. A. Harten, J. M. Hyman, and P. D. Lax, On finite difference approximations and entropy conditions for shocks, *Comm. Pure Appl. Math.* **29**, 297 (1976).
28. P. D. Lax and C. D. Levermore, The small dispersion limit of the Korteweg–Devries equation, 1, *Comm. Pure Appl. Math.* **36**, 253 (1983).
29. P. Maracati and R. Natalini, Convergence of the pseudo-viscosity approximation for conservation laws, *Nonlinear Anal. Theory Methods Appl.* **23**, 621 (1994).
30. M. L. Wilkins, Use of artificial viscosity in multidimensional fluid dynamic calculations, *J. Comput. Phys.* **36**, 281 (1980).
31. P. R. Woodward, Piecewise-parabolic methods for astrophysical fluid dynamics, in *Astrophysical Radiation Hydrodynamics*, edited by K.-H. A Winkler and M. L. Norman (Reidel, Dordrecht, 1986), p. 245.
32. M. J. Berger and P. Colella, Local adaptive mesh refinement for shock hydrodynamics, *J. Comput. Phys.* **82**, 64 (1989).
33. A. Harten, P. D. Lax, and B. van Leer, On upstream differencing and Godunov-type schemes for hyperbolic conservation laws, *SIAM Rev.* **25**, 35 (1983).